Lead in ancient Rome's city waters

Hugo Delile[a,b,1], Janne Blichert-Toft[b,c], Jean-Philippe Goiran[d], Simon Keay[e], and Francis Albarède[b,c]

[a]Université Lumière Lyon 2, Centre National de la Recherche Scientifique-Unité Mixte de Recherche (CNRS UMR) 5600, 69676 Bron, France; [b]Ecole Normale Supérieure de Lyon, Université Claude Bernard Lyon 1, CNRS UMR 5276, 69007 Lyon, France; [c]Department of Earth Science, Rice University, Houston, TX 77005; [d]Maison de l'Orient et de la Méditerranée, CNRS UMR 5133, 69365 Lyon Cedex 7, France; and [e]Archeology, Faculty of Humanities, University of Southampton, Southampton SO17 1BF, Great Britain

Edited by Thure E. Cerling, University of Utah, Salt Lake City, UT, and approved March 19, 2014 (received for review January 3, 2014)

It is now universally accepted that utilization of lead for domestic purposes and water distribution presents a major health hazard. The ancient Roman world was unaware of these risks. How far the gigantic network of lead pipes used in ancient Rome compromised public health in the city is unknown. Lead isotopes in sediments from the harbor of Imperial Rome register the presence of a strong anthropogenic component during the beginning of the Common Era and the Early Middle Ages. They demonstrate that the lead pipes of the water distribution system increased Pb contents in drinking water of the capital city by up to two orders of magnitude over the natural background. The Pb isotope record shows that the discontinuities in the pollution of the Tiber by lead are intimately entwined with the major issues affecting Late Antique Rome and its water distribution system.

harbor geoarcheology | paleopollution | Late Holocene | ore provenance | sedimentology

Statistics on demography, money supply and metal circulation, life and health standards, and many other social parameters required to understand modern history are largely missing from the written record of the ancient past. For example, the apparently simple question of how the population of ancient Rome evolved is still unresolved (1, 2), prompting the design of indirect estimates (3). Another well-publicized problem illustrating the lack of primary sources of accurate information is the decade-old debate on Pb poisoning of the high society of Rome, either by lead water pipes or grape juice concoctions prepared in lead cups (4–9). Here we focus on the condition of Pb in the public waters of ancient Rome. Lead is regarded as a powerful and ubiquitous indicator of the manufacturing status of a society. For example, a surge in Pb concentrations in the Greenland ice-core record was correlated with the height of the Roman Empire (10). Three out of the four existing Pb isotopes are rapidly modified by the radioactive decay of natural uranium or thorium over geological time. The mining of ores from geologically diverse areas produces metallic Pb with variable isotopic abundances that depend on the tectonic age and the Th/U and U/Pb ratios of the mining district. Archeologists interested in the provenance of artifacts routinely tap this wealth of information (11). To explore how the supply of metals from all over the Roman world and their utilization may have affected the nearby environment of ancient Rome, the present work sets out to investigate the isotope compositions of Pb in sediment cores from the Trajanic harbor basin at Portus, the maritime port of Imperial Rome, and the channel connecting Portus with the Tiber (Canale Romano) (Fig. S1). Harbors are excellent sedimentary traps. The record of human Pb pollution from the time that the harbor basin was excavated (*ca.* 112 AD) and well into the Middle Ages offers a new historical, *ca.* 1,000 y-long perspective on the evolution of Pb released by Rome, its water distribution system, and the major disruptive events that affected the life of the capital city and its harbor.

In 42 AD Claudius started the construction of an open coastal port to compensate for the long-standing shortcomings of the existing system for supplying Rome from the Mediterranean, notably the small scale of the harbor and anchorage facilities at Ostia and the long route of communication with the principal maritime port at Puteoli (Pozzuoli) on the Bay of Naples (12). The inland ~0.4 km^2 Trajanic basin, which was excavated in the early years of the second century AD in response to the growing demands of an expanding population in Rome, offered both safe mooring to sea-going merchant ships and immense warehouses and other buildings (13–15). Communication between the Claudian and Trajanic basins was facilitated by an entrance channel, into which the *ca.* 9-m-long core TR14 was drilled. Up until the Middle Ages, the Trajanic basin was also accessed from a man-made branch of the Tiber (Fossa Traiana; what is now the Fiumicino Canal) by means of the Canale Traverso. The transport of sand and silt sediments from this channel to the Trajanic Harbor has been attested to by sedimentological, geochemical, and ostracod analyses (16–18). The now filled-in Canale Romano, which ran past the southwestern side of the Trajanic basin toward the Tiber, was used to carry cargoes transshipped on to river-going craft bound for Rome (15). A 13-m-long core labeled CN1 was drilled into the sediments of the Canale Romano. The detailed sedimentology and geochemistry of core TR14 are given elsewhere together with ^{14}C ages (18). Some ^{14}C dates likewise were obtained for core CN1 (Table S1). For reference and modeling purposes, the bedload of the modern Tiber between Rome and the Tiber delta was also sampled (Table S2), as were five different Roman Pb water pipes (*fistulæ*) collected in Rome and dating to between the first and the second centuries AD (Fig. S2). In all, 42 samples from TR14, 37 samples from CN1, 6 samples from the Tiber bedload, and 10 samples from the five Roman *fistulæ* were measured for their Pb isotope compositions at the Ecole Normale Supérieure de Lyon.

Significance

Thirty years ago, Jerome Nriagu argued in a milestone paper that Roman civilization collapsed as a result of lead poisoning. Clair Patterson, the scientist who convinced governments to ban lead from gasoline, enthusiastically endorsed this idea, which nevertheless triggered a volley of publications aimed at refuting it. Although today lead is no longer seen as the prime culprit of Rome's demise, its status in the system of water distribution by lead pipes (*fistulæ*) still stands as a major public health issue. By measuring Pb isotope compositions of sediments from the Tiber River and the Trajanic Harbor, the present work shows that "tap water" from ancient Rome had 100 times more lead than local spring waters.

Author contributions: H.D., J.B.-T., J.-P.G., S.K., and F.A. designed research; H.D., J.B.-T., and J.-P.G. performed research; J.B.-T. contributed new reagents/analytic tools; H.D. and F.A. analyzed data; and H.D., J.B.-T., and F.A. wrote the paper.

The authors declare no conflict of interest.

This article is a PNAS Direct Submission.

[1]To whom correspondence should be addressed. E-mail: hdelile@gmail.com.

This article contains supporting information online at www.pnas.org/lookup/suppl/doi:10.1073/pnas.1400097111/-/DCSupplemental.

Results and Discussion

The TR14 core can be broken down into successive sedimentary units corresponding to different time slices: (*i*) preharbor up to *ca.* 100 AD, (*ii*) Early Empire up to *ca.* 250 AD, (*iii*) Late Empire up to *ca.* 500 AD, (*iv*) Early Middle Ages up to *ca.* 800 AD, and (*v*) Late Middle Ages (see the "Historical period age-depth model" columns in Fig. 1). Age boundaries between units may be uncertain by up to 100 y. Silts and sands dominate sediment mineralogy. The preharbor sequence attests to deposition in an environment of deltaic progradation (19). The construction of the harbor brings about a sharp sedimentological change and marks the beginning of the harbor mud deposits. A well-stratified ~50-cm-thick layer within the Early Empire deposits (753 cm) displaying well-preserved shells does not appear in other cores and may signal local dredging (18, 20). The layer corresponding to the Early Middle Ages contains more carbonates and ostracods of brackish affinity than the rest of the core. At the top, the sediments from the Late Middle Ages horizon are characteristic of flood plain deposits (17, 18).

In Fig. 1, two different representations of lead isotope variations in TR14 and CN1 have been used: First (Fig. 1*A*), the conventional raw isotopic ratios in which ^{206}Pb is kept as the denominator; and, second (Fig. 1*B*), a derived set of geologically informed parameters which will now be explained. In compliance

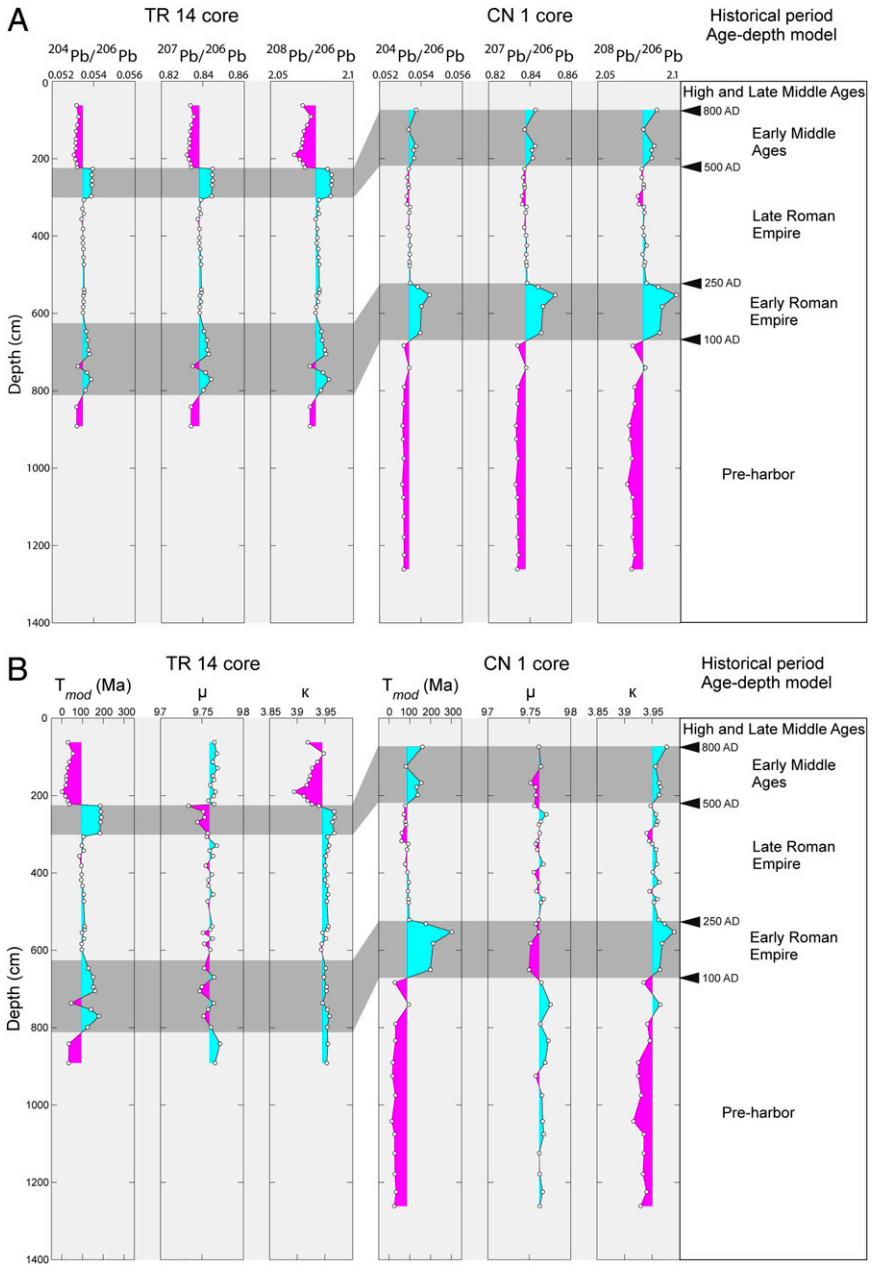

Fig. 1. Chronostratigraphic evolution of (*A*) the raw isotopic ratios of the cores TR14 and CN1 and (*B*) the geological parameters T_{mod}, $^{238}U/^{204}Pb$ (μ), and $^{232}Th/^{238}U$ (κ) derived from the raw isotope ratios as described in the main text. The different time slice boundaries (indicated with black arrowheads and highlighted by alternating light and dark gray shading for better visibility) derived from the age-depth model of core TR14 (18) coincide with major Pb isotope compositional shifts prominent in both cores. Hercynian Pb shows up during the Early Roman Empire and Early Middle Ages. In contrast, low-Th/U natural Pb dominates both the preharbor sequence and the flood plain deposits at the top of TR14.

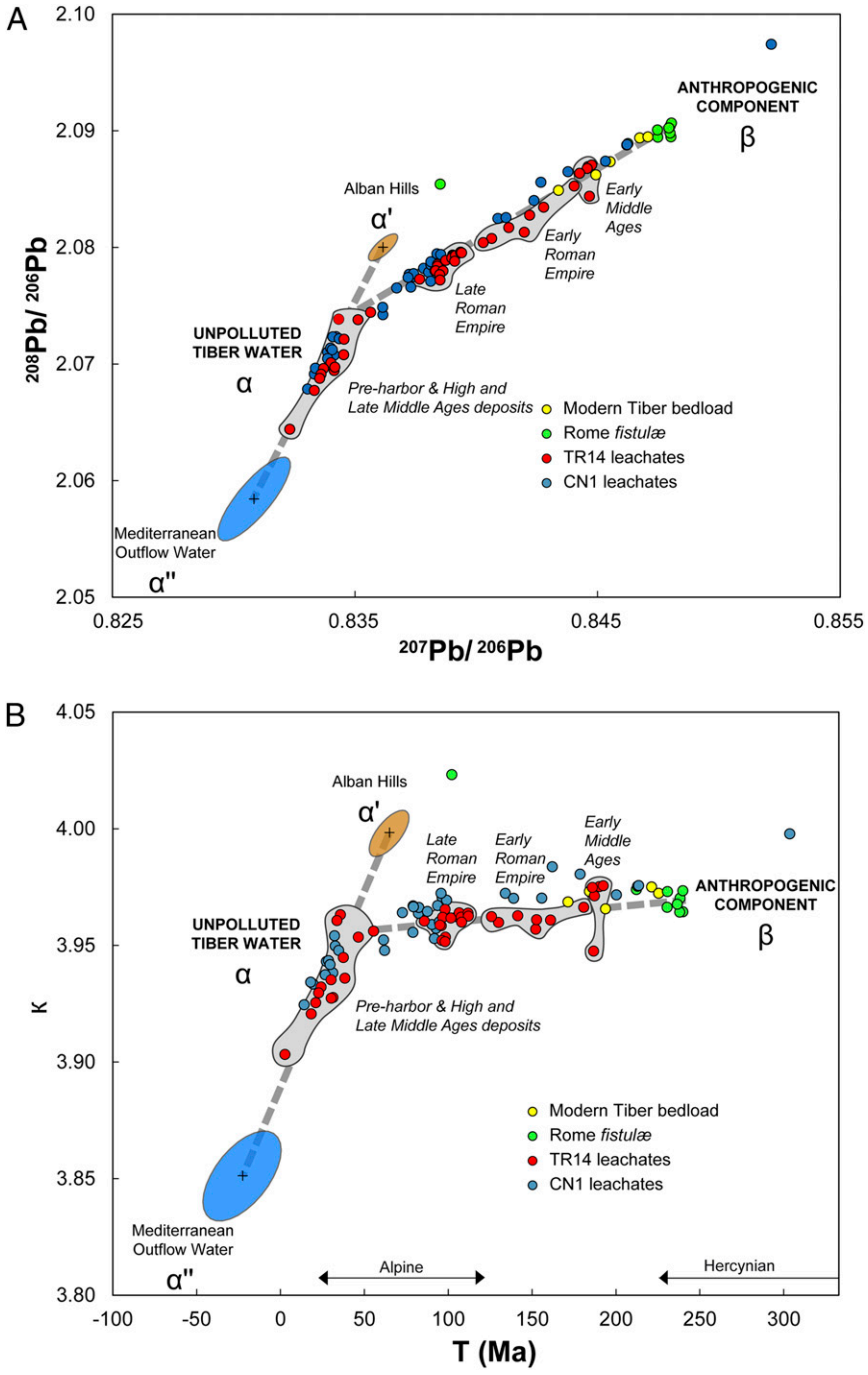

Fig. 2. (*A*) Lead isotope ratios ($^{207}Pb/^{206}Pb$ vs. $^{208}Pb/^{206}Pb$) and (*B*) geological parameters (κ vs. T_{mod}) for the leached samples from cores TR14 (red) and CN1 (blue), the modern Tiber bedload (yellow), and Rome *fistulæ* (green). The gray fields correspond to the light and dark gray shaded time slice bands of Fig. 1 and overlap the samples from core TR14 in accordance with the respective historical periods. The two mixing lines (gray dashes) connect, respectively, α and β on the one hand, and α′ and α″ on the other. The α end-member corresponds to unpolluted Tiber water and is composed of the Mediterranean outflow water (α″, blue ellipse) (30) and volcanic rocks from the Alban Hills (α′, orange ellipse) (28, 29). β is the anthropogenic end-member.

with literature (e.g., ref. 21), we searched Pb isotope databases for potential sources of ores matching the Pb isotope compositions of archeological artifacts and sediment samples (Fig. S3). In addition, the geological province to which a particular Pb sample belongs can often be inferred from a conversion of its isotope compositions into a set of geologically informed parameters, the Pb model age T_{mod}, and the apparent $^{238}U/^{204}Pb$ (μ) and $^{232}Th/^{238}U$ (κ) ratios (e.g., refs. 22–24). T_{mod} reflects the tectonic age of the crustal segments in which ore deposits occur. In Europe, crustal segments of Alpine ages (30–120 Ma) contrast with Hercynian (240 Ma and older) and early Paleozoic (>450 Ma) segments. μ and κ are parameters that tend to increase with crustal depth. Typically, κ is higher in crustal segments that lost their shallow levels by erosion or tectonic denudation, such as in Iberia, southern France, and the eastern Alps. Fig. S4 shows that these parameters can be used to divide Europe into coherent regions, which justifies using T_{mod}, μ, and κ for provenance purposes (24–26). T_{mod}, μ, and κ in turn provide a rapid characterization of the geological environment in which the ores formed. Ores formed by remobilization of metal from the underlying basement and hosted in sediments, such as Mississippi Valley type deposits, may to some extent challenge a simple interpretation of model ages. Fig. S4 shows, however, that, overall, the connection between Pb model ages and the tectonic age of the local crystalline basement remains very strong. The broad relationship between T_{mod}, μ, and κ tectonic provinces is compelling and holds particularly true for southern Europe (27).

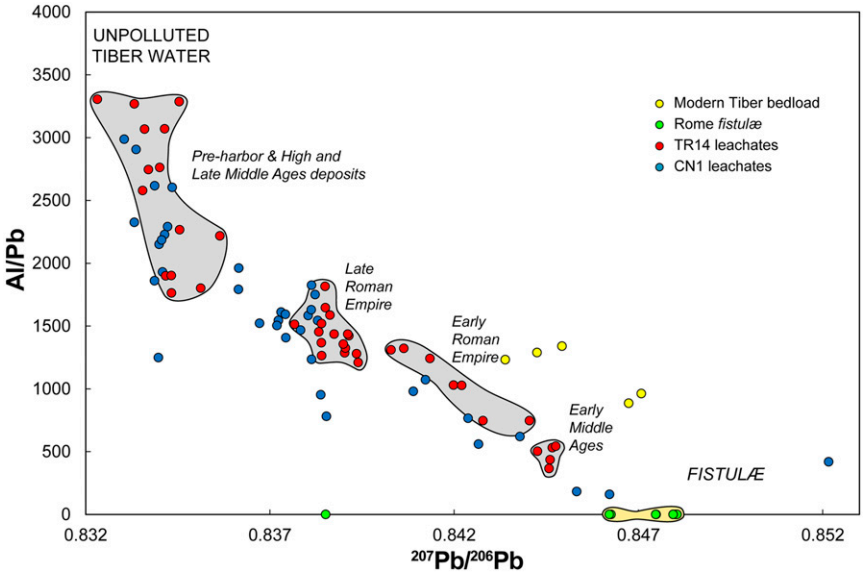

Fig. 3. Al/Pb vs. $^{207}Pb/^{206}Pb$ showing the TR14 (red) and CN1 (blue) core leachates, the modern Tiber bedload (yellow), and the Rome *fistulæ* (green). The beige field corresponds to the anthropogenic component characterized by the *fistulæ*. Symbols and parameters are as in Fig. 2. This plot shows that the Al-free, and therefore suspension-free, water component has the same Pb isotope composition as the *fistulæ* and therefore corresponds to clear water from the city water distribution system.

Principal component analysis of the 3D Pb isotopic data shows that >99% of the variance is accounted for by two principal components and, therefore, that the data plot in a plane spanning any 3D space of Pb isotopic ratios. Cores TR14 and CN1 define indistinguishable planes, which allows the Pb isotope data to be merged into a single dataset. As illustrated by the $^{208}Pb/^{206}Pb$ vs. $^{207}Pb/^{206}Pb$ plot of Fig. 2*A*, the isotope composition of Pb in leachates form two coplanar alignments, which are most straightforwardly accounted for by the mixing of components of different origins.

In Fig. 2 *A* and *B*, the component labeled α located at the intersection (the kink) of the two trends is ubiquitous in both cores including the preharbor and Late Middle Ages deposits. It is also an end-member in plots of Pb isotope ratios from leaching residues (Fig. S5 *A* and *B*). This component therefore reflects Pb naturally present in Tiber water. It can itself be broken down into a mixture of two local low-$^{207}Pb/^{206}Pb$ sources, the component α′ originating from the recent volcanic rocks of the Alban Hills (28, 29), and the component α″, which is very similar to Pb dissolved in modern Mediterranean seawater (30) and released by erosion of recent limestones from the Apennines.

The anthropogenic nature of the third component β becomes apparent when plotting Al/Pb (data from ref. 18) as a function of $^{207}Pb/^{206}Pb$ (Fig. 3). The α–β alignment intersects the *x* axis at the value of $^{207}Pb/^{206}Pb$ of the *fistulæ* (Al/Pb ≈0), which shows that the contaminant is essentially pure lead from Al-free and therefore suspension-free water. As with raw isotopic ratios, a plot of κ vs. T_{mod} (Fig. 2*B*) shows a bundle of alignments consistent with the observations from isotopic ratios. The alignment trending toward high $^{207}Pb/^{206}Pb$ and old model ages reveals that Pb component β is of Hercynian (or Variscan; T_{mod} ≈250 Ma) affinity with rather high κ values. Hercynian Pb is absent from peninsular Italy, and the Apennines formed less than 20 Ma ago (31) from recent sediments and volcanic rocks. The Pb component β therefore, clearly being foreign to peninsular Italy, should rather be traced to southwestern Spain, the Massif Central of France, the eastern Alps, Eifel in Germany, the Pennines in England, and Macedonia (Fig. S3). Among these potential sources, only some of them are consistent with the known maritime freight routes, which are punctuated by frequent shipwrecks loaded with Pb ingots (32–34), and with the known period and output of mine exploitation during the Late Republican Period and the Early Roman Empire (e.g., refs. 21 and 35). An unexpected observation is the lack of signal from the productive and geologically young mining areas of the Spanish Betics (Carthagene). It is most likely that the Pb used for water management in Rome had been mined in the Spanish Sierra Morena, the English Pennines, the German Eifel, or the French Massif Central.

The isotope composition of component β is remarkably consistent with the data on four of the five lead *fistulæ* analyzed in this work. Component β is still conspicuous in the leachates from the modern Tiber bottom sediments, which suggests that to this day old Pb pollution still permeates the bedload sediment. The anthropogenic origin of the Hercynian Pb component β is also attested to by the comparison of leachates and residues: $^{207}Pb/^{206}Pb$ is, with the sole exception of the deepest sample, higher in leachates than in residues (Fig. 4). Leaching therefore releases older labile Pb from a solid residue of much younger geological age.

Lead pollution of the Tiber River can be evaluated in a simple way by using

$$\varphi_{fist} = \frac{(^{207}Pb/^{206}Pb)_{riv} - (^{207}Pb/^{206}Pb)_{nat}}{(^{207}Pb/^{206}Pb)_{fist} - (^{207}Pb/^{206}Pb)_{nat}},$$

where φ_{fist} is the fraction of Pb in river water derived from Pb *fistulæ*. It has been estimated that the proportion f_{fist} of Tiber water running through the aqueducts was about 3% at the peak of the Roman Empire (36). It can therefore be deduced that *fistulæ* increased Pb in the water distributed in Rome over the natural level by a factor of about 40, 14, and 105 for the Early Empire, Late Empire, and High Middle Ages, respectively (*SI Materials and Methods*). Although the value of f_{fist} is only an educated guess pertinent to a given period, using different numbers does not significantly affect the relative levels of Pb pollution deduced. These levels are maximum values because they characterize the final output of the water system to the Tiber while most Roman citizens would have used drinking water that was tapped, whether legally or illegally, all along the water distribution system (36). The inferred increases of Pb in the water of the Roman distribution system unquestionably attest to general lead pollution of Roman drinking water but the Pb concentrations at issue are unlikely to have represented a major health risk (9).

Evidence bearing on the timeline of anthropogenic pollution in the Rome area can be derived from the sequence of Pb isotope characteristics (Fig. 2). Lead in preharbor sediments is of

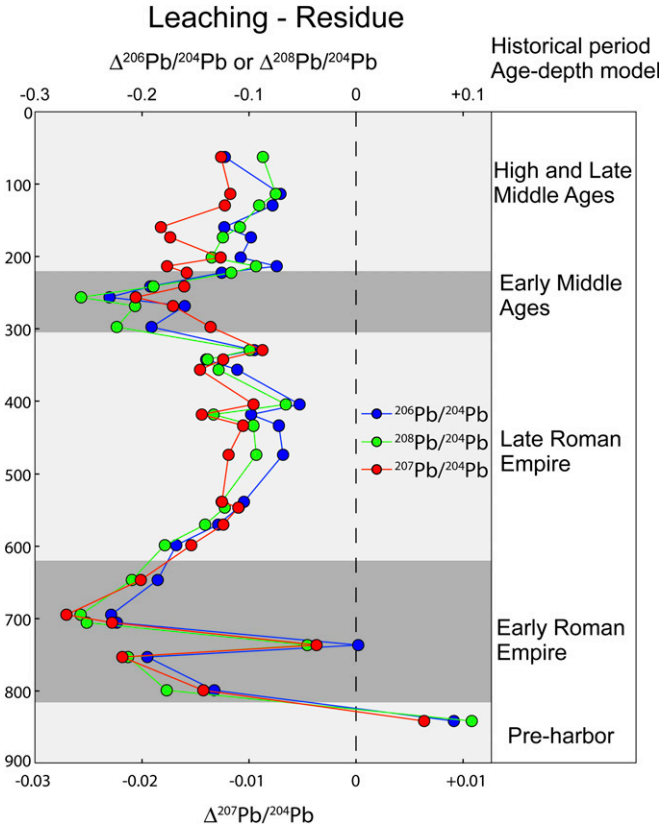

Fig. 4. TR14 downcore behavior of the isotopic contrast (ΔPb isotope ratios) between the residue and the leachate. Increasing distance from the zero dashed line (left side of the figure) indicates increasingly predominant anthropogenic impact, which is strongest during the Early Roman Empire and the Early Middle Ages. Time slice model as in Fig. 1.

natural origin (trend α′–α″). Excavation of basin deposits dating to the period of the Early Roman Empire coincides with both a surge of Hercynian Pb in leachates and a dramatic drop in the isotopic contrast between the residue and the leachate (trend α–β) (Fig. 4). At this time, the Roman Empire reached the height of its conquests, especially in western European territories such as Britain (Fig. S3). The isotopic contrast between the fractions rapidly diminishes, although quite smoothly, from the Early to the Late Roman Imperial periods. This change is largely accounted for by the dramatically smaller contribution of anthropogenic Pb to leachates and therefore by a lesser pollution of Tiber water. One interpretation of this may be a redirection of spring water away from the lead pipes of Rome, in some way related to the controversial decline of the population (3, 37) or to a poorly documented deterioration of the water distribution system.

At the end of the Late Roman Empire and throughout the Early Middle Ages section of TR14, the isotopic difference between the leachate and the residue bounces back and the presence of a rather homogenous anthropogenic component rich in Hercynian Pb again becomes prevalent in leachates (Figs. 2 and 4). The discontinuity appears in both the TR14 and CN1 cores (Fig. 1). The end of the Early Middle Ages section (~800 AD) is also brutal and signals the return of uncontaminated Pb in the Tiber (trend α′–α″). The persistence of Hercynian Pb in the bedload of the modern Tiber nevertheless indicates that centuries of contamination, possibly in the form of Pb carbonates, left a lasting imprint on the river sediments.

The consistency of the Pb isotope results from the CN1 core, which is expected to carry a straightforward Tiber signal, with those from the TR14 core is rather good despite the latter being susceptible to both harbor activity and input of water from the Portus aqueduct, which has its source in the vicinity of modern Ponte Galeria. Both cores reflect the presence of a Hercynian endmember and coincide on the timing of major isotopic shifts. κ values in the CN1 core may, however, be marginally higher than those in TR14, especially during the Early Empire. It is unfortunate that the Pb isotope database on pipes used for water distribution is still too limited to identify such small differences with confidence.

The extensive nature of the harbor installations calls for additional work beyond the 95 samples of sediment core, bedload, and Pb pipes from Portus and the Tiber analyzed in this study to demonstrate unambiguously that the observed discontinuities in the Pb isotope and overall geochemical record correspond to catastrophic disruptions of Portus activity. Although the coastal position of the port leaves the Trajanic basin vulnerable to river vagaries and maritime hazards, the lack of coarse gravels and sediment sorting, combined with the good preservation of the delicate ostracod shells, are strong evidence against exceptional floods, storms, and tsunamis. The age-depth model (18) is certainly evocative of some critical dates of Roman history. As speculated by Delile et al. (18) based on the ^{14}C record of TR14 and adjacent cores, transitions between units may be correlated with the initial excavation of the Trajanic basin (by *ca.* 112 AD), the continued use of the port during the third century (*ca.* 250 AD), the gradual fortification and contraction of the port in the later fifth and earlier sixth centuries (*ca.* 500 AD), and the transition to the post-Byzantine period. The later fifth and sixth century transition is coeval with Belisarius' fixing of the decommissioned aqueducts of Rome (38) at the end of the Gothic Wars (535–554 AD). Byzantine repairs of the water distribution system may have remobilized massive amounts of corrosion products from abandoned lead pipes in which water may have stagnated for protracted lengths of time. Although a causal relationship cannot be formally demonstrated, the discontinuities in the cores at Portus seem contemporaneous with historically documented events such as the struggle for the control of the port between Gothic and Byzantine forces (536–552 AD) and the damages inflicted to the water distribution system during the Arab sack of Rome in the mid-ninth century. Further work is needed to learn whether the causes of Portus' demise were natural, with the harbor finally falling into disuse on account of flood plain deposits, possibly after the major floods of 856 AD (39–41), or a consequence of military events (39).

Conclusions

This work has shown that the labile fraction of sediments from Portus and the Tiber bedload attests to pervasive Pb contamination of river water by the Pb plumbing controlling water distribution in Rome. Lead pollution of "tap water" in Roman times is clearly measurable, but unlikely to have been truly harmful. The discontinuities punctuating the Pb isotope record provide a strong background against which ideas about the changing character of the port can be tested.

Materials and Methods

After removal of the coarse gravel fraction, 500 mg of sample were crushed and treated with chloroform to remove most of the abundant organic fraction. The residue was rinsed and leached in dilute HBr. Because lead pipe corrosion products, such as Pb carbonates (42, 43), were suspected to be present in the sediments and carry a signal from aqueducts, no attempt was made at using the more specific protocols developed to selectively extract hydroxide coatings (e.g., ref. 44). Lead from the leachates was purified on an ion exchange resin using HBr as eluent of the sample matrix and HCl to elute Pb. The amounts of Pb extracted were large (>1 μg) and orders of magnitude above the blank of the procedure (~20 pg). Lead isotope compositions were analyzed by multicollector inductively-coupled plasma mass spectrometry on both the residues and the leachates of the samples from TR14 and the results were so systematic that no further attempt was made to also measure the residues from CN1 (Table S2).

ACKNOWLEDGMENTS. We thank the Soprintendenza Speciale per i Beni Archeologici di Roma: P. Catalano, L. Cianfriglia, A. Pellegrino, L. Vendittelli (Director of the Crypta Balbi Museum), M. Piranomonte, and Lorenza Manfredi (Istituto di Studi sulle Civiltà Italiche e del Mediterraneo Antico) for providing samples of Roman lead pipes from the water distribution system of ancient Rome. We also thank J.-P. Bravard, J.-C. Domergue, and R. Macchiarelli for helpful advice; two anonymous referees for constructive remarks; and the Institut National des Sciences de l'Univers for supporting the analytical facility at École Normale Supérieure de Lyon and P. Telouk for ensuring that instruments were always at their best. We acknowledge the Accélérateur pour la Recherche en sciences de la Terre, Environnement, Muséologie, Implanté à Saclay program for carrying out the accelerator mass spectrometry radiocarbon dating. We also acknowledge the École Française de Rome, the British School at Rome, the University of Southampton (The Portus Project), the Soprintendenza Speciale per I Beni Archeologici di Roma, the Young Scientist Program of the Agence Nationale de la Recherche, and the Centre National de la Recherche Scientifique–Institut des sciences humaines et sociales/Institut écologie et environnement (Action Interdisciplinaire de Recherche Archéométrie and Homere Project) for their financial and logistical support.

1. Lo Cascio E (1994) The size of the Roman population: Beloch and the meaning of the Augustan census figures. *JRS* 84:23–40.
2. Scheidel W (2008) *People, Land, and Politics: Demographic Developments and the Transformation of Roman Italy, 300 BC - AD 14*, eds De Light S, Northwood SJ (Brill, Leiden, The Netherlands), pp 17–70.
3. Turchin P, Scheidel W (2009) Coin hoards speak of population declines in Ancient Rome. *Proc Natl Acad Sci USA* 106(41):17276–17279.
4. Nriagu JO (1983) *Lead and Lead Poisoning in Antiquity* (John Wiley & Sons, New York).
5. Hodge AT (1981) Vitruvius, lead pipes and lead poisoning. *Am J Archaeol* 85(4): 486–491.
6. Scarborough J (1984) The myth of lead poisoning among the Romans: An essay review. *J Hist Med Allied Sci* 39(4):469–475.
7. Patterson CC, Shirahata H, Ericson JE (1987) Lead in ancient human bones and its relevance to historical developments of social problems with lead. *Sci Total Environ* 61:167–200.
8. Aufderheide AC, et al. (1992) Lead exposure in Italy: 800 BC-700 AD. *Int J Anthropol* 7(2):9–15.
9. Retief FP, Cilliers L (2006) Lead poisoning in ancient Rome. *Acta Theologica* 26(2): 147–164.
10. Hong S, Candelone J-P, Patterson CC, Boutron CF (1994) Greenland ice evidence of hemispheric lead pollution two millennia ago by Greek and Roman civilizations. *Science* 265(5180):1841–1843.
11. Stos-Gale ZA, Gale NH (2009) Metal provenancing using isotopes and the Oxford archaeological lead isotope database (OXALID). *Archaeol Anthropol Sci* 1(3):195–213.
12. Goiran J-P, et al. (2014) Geoarchaeology confirms location of the ancient harbour basin of Ostia (Italy). *J Archaeol Sci* 41:389–398.
13. Juvenal (1974) *Saturae* [Satires] (Les Belles Lettres, Paris).
14. Lugli G, Filibeck G (1935) Il porto di Roma imperiale e l'agro portuense [The Harbor of Imperial Rome and the Agro Portuense] (Officine dell'Istituto Italiano d'Arti Grafiche, Rome).
15. Keay S, Millett M, Paroli L, Strutt K (2005) *Portus: An Archaeological Survey of the Port of Imperial Rome* (British School at Rome, London).
16. Goiran J-P, et al. (2010) Palaeoenvironmental reconstruction of the ancient harbors of Rome: Claudius and Trajan's marine harbors on the Tiber delta. *Quat Int* 216(1–2): 3–13.
17. Salomon P, Delile H, Goiran J-P, Bravard J-P, Keay S (2012) The Canale di Comunicazione Traverso in *Portus*: The Roman sea harbour under river influence (Tiber Delta, Italy). *Géomorphologie* 1:75–90.
18. Delile H, et al. (2014) Geochemical investigation of a sediment core from the Trajan basin at *Portus*, the harbor of ancient Rome. *Quat Sci Rev* 87:34–45.
19. Bellotti P, et al. (2011) The Tiber river delta plain (central Italy): Coastal evolution and implications for the ancient Ostia Roman settlement. *Holocene* 21(7):1105–1116.
20. Sadori L, Giardini M, Giraudi C, Mazzini I (2010) The plant landscape of the imperial harbour of Rome. *J Archaeol Sci* 37(12):3294–3305.
21. Bode M, Hauptmann A, Mezger K (2009) Tracing Roman lead sources using lead isotope analyses in conjunction with archaeological and epigraphic evidence—a case study from Augustan/Tiberian Germania. *Archaeol Anthropol Sci* 1(3):177–194.
22. Moorbath S (1962) Lead isotope abundance studies on mineral occurrences in the British Isles and their geological significance. *Phil Trans R Soc A* 254(1042):295–360.
23. Pernicka E, Begemann F, Schmitt-Strecker S, Wagner GA (1993) Eneolithic and Early Bronze Age copper artefacts from the Balkans and their relation to Serbian copper ores. *Prähist Z* 68(1):1–54.
24. Albarède F, Desaulty A-M, Blichert-Toft J (2012) A geological perspective on the use of Pb isotopes in Archaeometry. *Archaeometry* 54(5):853–867.
25. Desaulty A-M, Telouk P, Albalat E, Albarède F (2011) Isotopic Ag-Cu-Pb record of silver circulation through 16th-18th century Spain. *Proc Natl Acad Sci USA* 108(22): 9002–9007.
26. Desaulty A-M, Albarede F (2013) Copper, lead, and silver isotopes solve a major economic conundrum of Tudor and early Stuart Europe. *Geology* 41(2):135–138.
27. Arribas A, Tosdal RM (1994) Isotopic composition of Pb in ore deposits of the Betic Cordillera, Spain; origin and relationship to other European deposits. *Econ Geol* 89(5):1074–1093.
28. Conticelli S, D'Antonio M, Pinarelli L, Civetta L (2002) Source contamination and mantle heterogeneity in the genesis of Italian potassic and ultrapotassic volcanic rocks: Sr–Nd–Pb isotope data from Roman Province and Southern Tuscany. *Mineral Petrol* 74(2–4):189–222.
29. D'Antonio M, Tilton GR, Civetta L (1996) Petrogenesis of Italian alkaline lavas deduced from Pb-Sr-Nd isotope relationships. *Earth Processes: Reading the Isotopic Code*, Monograph Series, eds Basu A, Hart S (American Geophysical Union, Washington), pp 253–267.
30. Stumpf R, Frank M, Schönfeld J, Haley BA (2010) Late Quaternary variability of Mediterranean Outflow Water from radiogenic Nd and Pb isotopes. *Quat Sci Rev* 29(19–20):2462–2472.
31. Faccenna C, Becker TW, Lucente FP, Jolivet L, Rossetti F (2001) History of subduction and back-arc extension in the Central Mediterranean. *Geophys J Int* 145(3):809–820.
32. Domergue C, Quarati P, Nesta A, Obejero G, Trincherini PR (2012) Les isotopes du plomb et l'identification des lingots de plomb romains des mines de Sierra Morena. Questions de méthode: l'exemple des lingots de l'épave Cabrera 4. *Pallas* 90: 243–256.
33. Brown HG (2011) A study of lead ingot cargoes from ancient Mediterranean shipwrecks. MA dissertation (Texas A&M Univ, College Station, TX).
34. Robinson D, Wilson A, eds (2011) *Maritime Archaeology and Ancient Trade in the Mediterranean* (Oxford Centre for Maritime Archaeology, Oxford).
35. Domergue C (2008) *Les mines antiques: La production des métaux aux époques grecque et romaine* [Ancient Mines: Metal Production During the Greek and Roman Eras] (Picard, Paris).
36. Blackman DR, Hodge AT (2001) *Frontinus' Legacy* (Univ of Michigan Press, Ann Arbor, MI).
37. Lo Cascio E (2001) *La population* [The population]. *Pallas* 55:179–198.
38. Procopius *History of the Wars*, trans Dewing HB, Heinemann W (1962) (Harvard Univ Press, Cambridge, MA).
39. Duchesne L (1955) Le Liber pontificalis: Texte, introduction et commentaire [The Liber Pontificalis: Text, Introduction, and Commentary], ed Vogel C (E. de Boccard, Paris).
40. Lanciani R (1899) *The destruction of ancient Rome* (The Macmillan Company, New York).
41. Keay SJ (2011) *Portus and Its Hinterland: Recent Archaeological Research*, ed Paroli L (British School at Rome, London).
42. Grimes SM, Johnston SR, Batchelder DN (1995) Lead carbonate–phosphate system: Solid–dilute solution exchange reactions in aqueous systems. *Analyst (Lond)* 120(11): 2741–2746.
43. Peters NJ, Davidson CM, Britton A, Robertson SJ (1999) The nature of corrosion products in lead pipes used to supply drinking water to the City of Glasgow, Scotland, UK. *Fresenius'. J Anal Chem* 363(5–6):562–565.
44. Bayon G, et al. (2002) An improved method for extracting marine sediment fractions and its application to Sr and Nd isotopic analysis. *Chem Geol* 187(3–4):179–199.

Supporting Information

Delile et al. 10.1073/pnas.1400097111

SI Materials and Methods

Any Additional Author Notes. The following derives the equation in the main text relative to ancient Tiber pollution. Let us label "riv" the polluted Tiber water, "nat" the Tiber water upstream from Rome, and "fist" the water flowing in the aqueduct + *fistulæ* water distribution system. The following mass balance equation

$$\left(\frac{^{207}\mathrm{Pb}}{^{206}\mathrm{Pb}}\right)_{riv} = \varphi_{fist}^{\,^{206}\mathrm{Pb}}\left(\frac{^{207}\mathrm{Pb}}{^{206}\mathrm{Pb}}\right)_{fist} + \left(1-\varphi_{fist}^{\,^{206}\mathrm{Pb}}\right)\left(\frac{^{207}\mathrm{Pb}}{^{206}\mathrm{Pb}}\right)_{nat} \quad [S1]$$

in which

$$\varphi_{fist} = \frac{f_{fist}C_{fist}^{\,^{206}\mathrm{Pb}}}{f_{fist}C_{fist}^{\,^{206}\mathrm{Pb}} + \left(1-f_{fist}\right)C_{nat}^{\,^{206}\mathrm{Pb}}} \quad [S2]$$

is the fraction of ^{206}Pb present in Tiber water and contributed by the water distribution system, f is the fraction of water flowing through either pathway, and C refers to concentrations. As per the equation in the main text, φ_{fist} can be determined to be

$$1-\varphi_{fist} = \frac{\left(1-f_{fist}\right)C_{nat}^{\,^{206}\mathrm{Pb}}}{f_{fist}C_{fist}^{\,^{206}\mathrm{Pb}} + \left(1-f_{fist}\right)C_{nat}^{\,^{206}\mathrm{Pb}}}. \quad [S3]$$

Dividing **S2** by **S3** gives

$$\frac{C_{fist}^{\,^{206}\mathrm{Pb}}}{C_{nat}^{\,^{206}\mathrm{Pb}}} = \frac{\varphi_{fist}/\left(1-\varphi_{fist}\right)}{f_{fist}/\left(1-f_{fist}\right)}. \quad [S4]$$

If the fraction f_{fist} of the Tiber flow contributed by the water distribution system (3%) is known, the relative enrichment of the water distributed by *fistulæ* can be determined from **S4**.

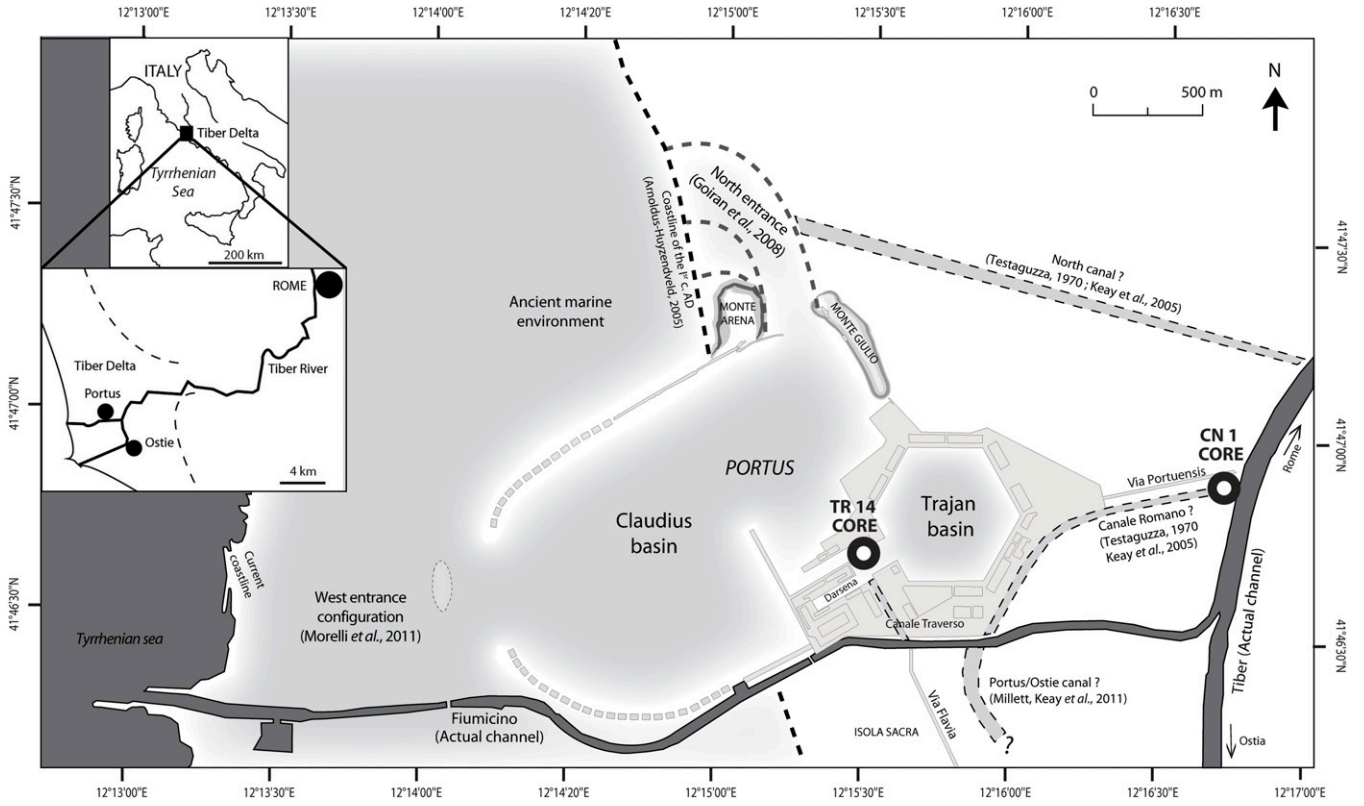

Fig. S1. Map of the Portus area with the Claudius and Trajan Harbors and connecting waterways showing the location of the cores TR14 and CN1 analyzed in this work.

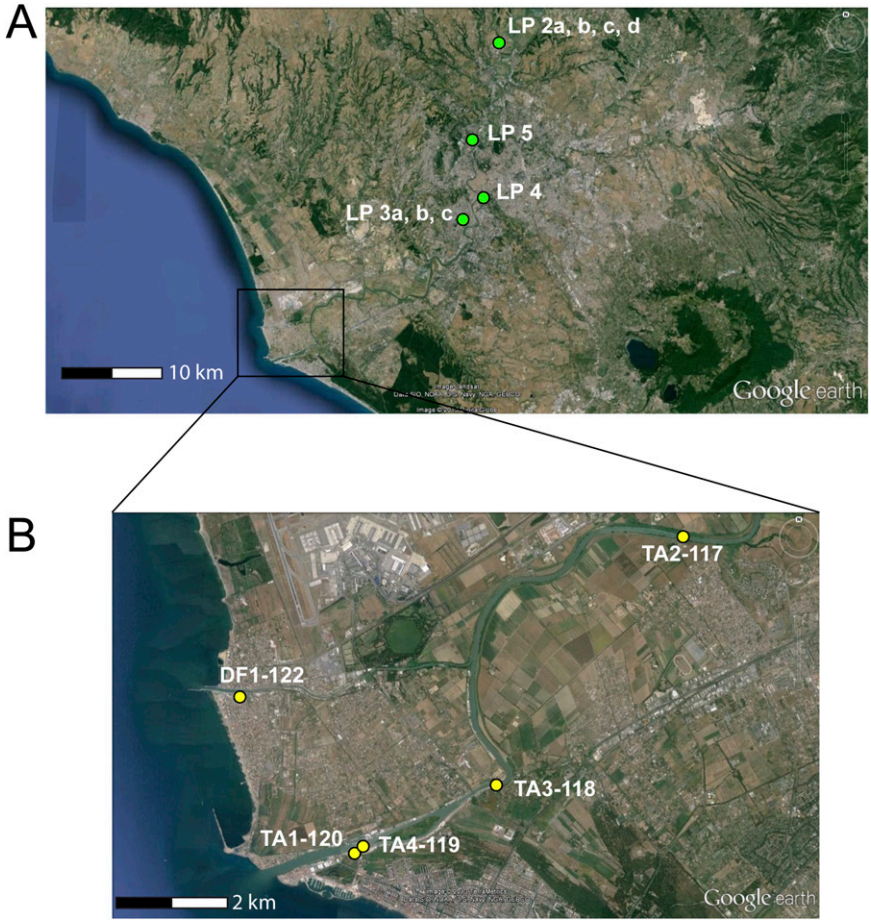

Fig. S2. Maps showing the locations of (*A*) the Roman lead pipes (*fistulæ*) and (*B*) the modern Tiber bedload samples. The precise location of the LP1 *fistulæ* is not known.

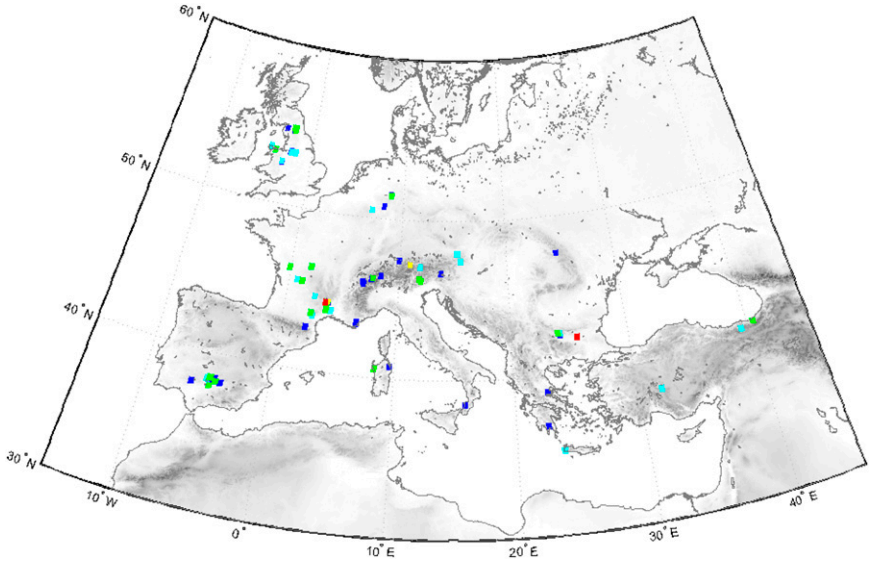

Fig. S3. Map of Europe showing pixels from the database that best agree with the raw Pb isotope compositions of the *fistulæ*. Squares correspond to potential sources for Pb used in the *fistulæ* of Rome's water distribution system. The mean value of $^{204}Pb/^{206}Pb$, $^{207}Pb/^{206}Pb$, and $^{208}Pb/^{206}Pb$ of *fistulæ* has been compared with the mean value of Pb ores in each individual $0.25° \times 0.25°$ pixel calculated from >6000 data held in our database. The request finds the pixels in the database for which the error-weighted Mahalanobis distance to the mean *fistulæ* composition in the space of Pb isotopes is minimum. Error weighted means that the metric is defined by the covariance matrix of analytical errors and the distance should be viewed as a generalization of the statistics underlying Student's *t* distribution to multivariate sample sets. The color code corresponds to distances of 2 (red), 4 (yellow), 6 (green), 8 (cyan), and 10 (blue) sigmas with one sigma equal to 0.15 per mil of the isotopic ratio value. Although two pixels color coded in red are identified in Bulgaria and the southeastern Massif Central, the historical record of mining and the routes identified by shipwrecks loaded with Pb ingots leave southwestern Spain, the English Pennines, the German Eifel, and the French Massif Central as the most probable sources of the Pb *fistulæ* of Rome.

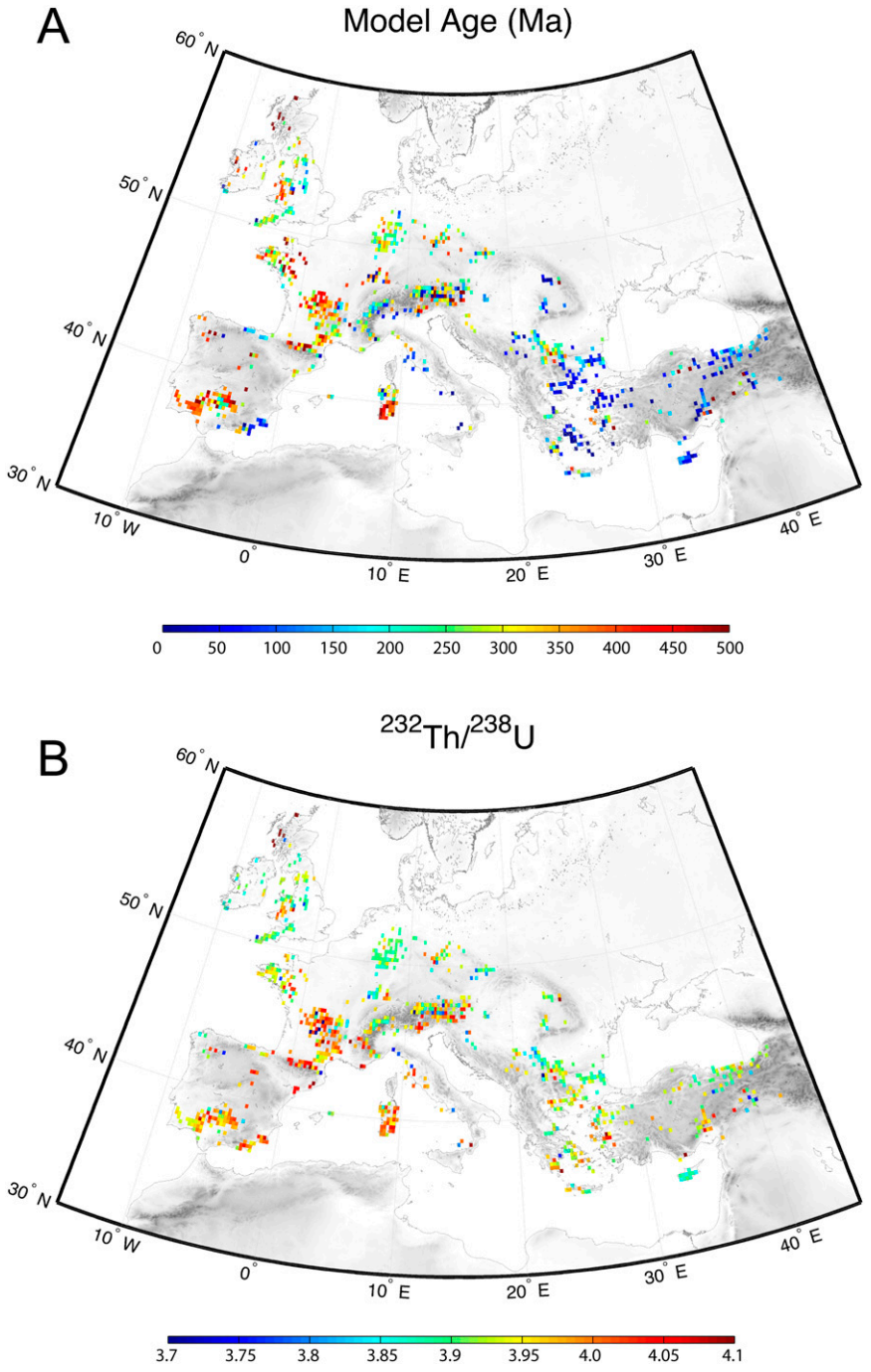

Fig. S4. Geolocalized database of Pb isotopic compositions in ores (>6,000 samples) with grid cells (pixels) of 0.25° × 0.25°. The map of Pb model ages (*A*) reflects the tectonic age of the crustal segments, whereas the map of $^{232}Th/^{238}U$ (κ) (*B*) reflects the crustal depth. The list of references can be obtained upon request from H.D.

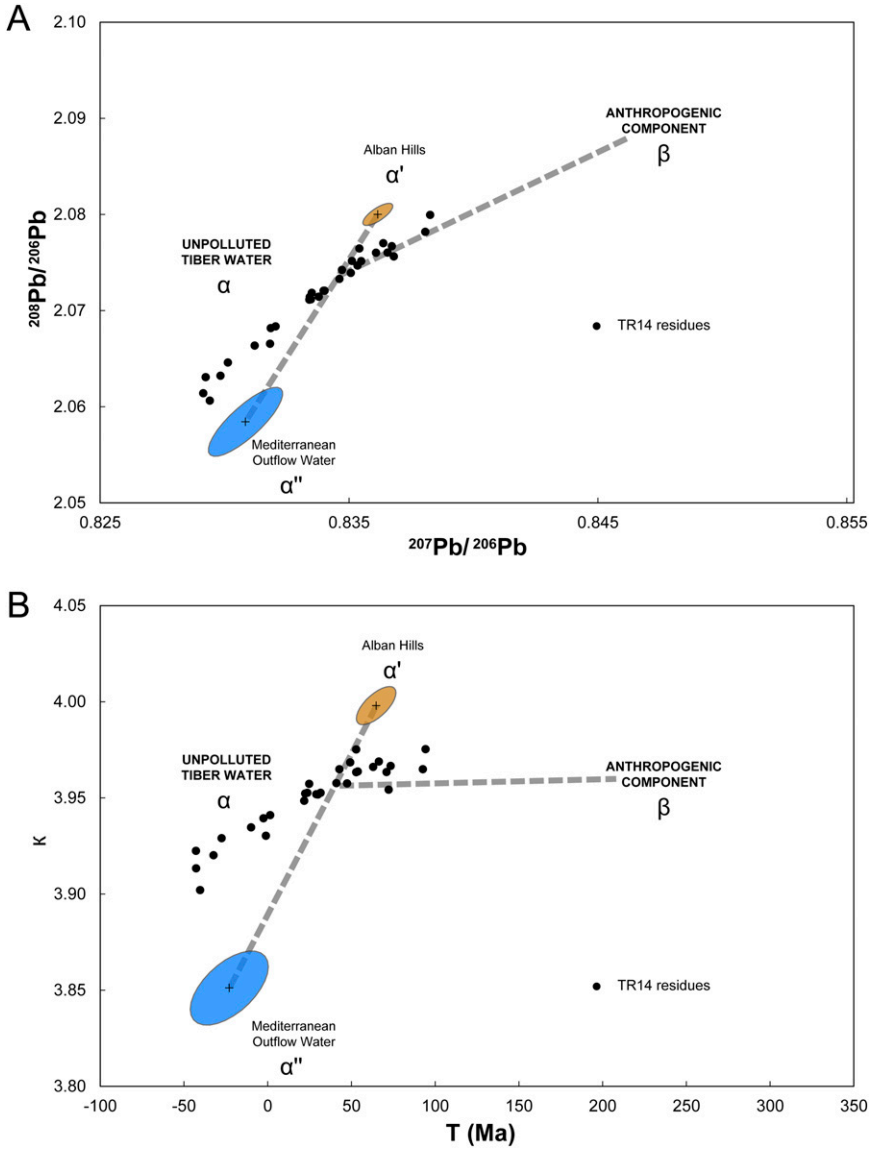

Fig. S5. (*A*) Lead isotope ratios ($^{207}Pb/^{206}Pb$ vs. $^{208}Pb/^{206}Pb$) and (*B*) geological parameters (κ vs. T_{mod}) for the residues from core TR14 (black circles). Other symbols and parameters are as in Fig. 2.

Table S1. ^{14}C dating of the cores TR14 and CN1

Core	Depth, cm	Laboratory code	Material	$\delta\ ^{13}C$	^{14}C age, B.P.	Calendar age, BC–AD; 2σ
TR 14	341–344	Lyon-7474	Vegetal matter*	−13.26	2,160 ± 30	97–284 AD
TR 14	341–344	Lyon-8067	*Posidonia**	−13.85	2,165 ± 25	104–266 AD
TR 14	403–406	Lyon-8068	*Posidonia**	−13.35	2,145 ± 25	130–305 AD
TR 14	432–435	Lyon-8069	*Posidonia**	−13.86	2,035 ± 25	265–426 AD
TR 14	549–549.5	Lyon-7470	Vegetal matter*	−13.41	2,140 ± 30	131–327 AD
TR 14	696–699	UCIAMS-114467	Wood	−24.7	1,790 ± 20	137–323 AD
TR 14	700–707	Lyon-8777	Wood	ND	1,765 ± 30	209–380 AD
TR 14	772–765	Lyon-8876	Wood	−25.43	1,710 ± 35	248–409 AD
TR 14	772–765	Lyon-8877	Charcoal	−26.31	2,080 ± 25	176–40 BC
TR 14	792–787	Lyon8776	*Posidonia**	ND	2,250 ± 30	12 BC–171 AD
CN 1	440–445	Lyon-8878	Wood	ND	1,545 ± 25	430–573 AD
CN 1	475–477	Lyon-8073	Charcoal	ND	1,650 ± 25	264–438 AD
CN 1	600–650	Lyon-6866	Bone	ND	1,915 ± 30	5–139 AD

ND, not determined.

*Ages were calibrated according to the IntCal09 and Marine09 radiocarbon calibration curves (1).

1. Reimer PJ, et al. (2009) IntCal09 and Marine09 radiocarbon age calibration curves, 0–50,000 years cal BP. *Radiocarbon* 51(4):1111–1150.

Table S2. Summary of the analytical data of this study (Pb isotopic compositions and geological parameters) for the TR14 and CN1 cores, modern Tiber bedload, and Rome *fistulæ*

Material	Code	Depth, cm	$^{208}Pb/^{204}Pb$	$^{207}Pb/^{204}Pb$	$^{206}Pb/^{204}Pb$	$^{207}Pb/^{206}Pb$	$^{208}Pb/^{206}Pb$	T_{mod}, Ma	μ	κ
Core TR14 leachate	34L	63	38.916	15.686	18.805	0.83414	2.06943	31.3	9.764	3.928
Core TR14 leachate	31L	92	38.940	15.686	18.771	0.83564	2.07443	55.5	9.767	3.956
Core TR14 leachate	20L	114	38.943	15.685	18.794	0.83455	2.07212	37.5	9.762	3.945
Core TR14 leachate	40L	130	38.940	15.688	18.811	0.83401	2.07011	30.2	9.768	3.935
Core TR14 leachate	3L	150	38.939	15.686	18.815	0.83370	2.06960	24.3	9.763	3.932
Core TR14 leachate	32L	160	38.937	15.687	18.818	0.83360	2.06911	22.8	9.764	3.930
Core TR14 leachate	21L	174	38.926	15.684	18.816	0.83355	2.06876	21.0	9.759	3.925
Core TR14 leachate	37L	190	38.913	15.689	18.850	0.83232	2.06439	2.7	9.765	3.903
Core TR14 leachate	22L	202	38.923	15.687	18.824	0.83332	2.06772	18.4	9.763	3.921
Core TR14 leachate	25L	214	38.910	15.682	18.800	0.83417	2.06972	30.3	9.757	3.927
Core TR14 leachate	41L	223	38.923	15.686	18.795	0.83454	2.07079	38.5	9.765	3.936
Core TR14 leachate	4L	227	38.636	15.657	18.536	0.84466	2.08438	186.7	9.733	3.948
Core TR14 leachate	42L	242	38.711	15.667	18.549	0.84461	2.08692	190.2	9.752	3.975
Core TR14 leachate	23L	257	38.708	15.667	18.546	0.84476	2.08705	192.4	9.753	3.976
Core TR14 leachate	5L	269	38.700	15.662	18.545	0.84458	2.08676	187.2	9.743	3.971
Core TR14 leachate	29L	298	38.723	15.670	18.560	0.84426	2.08635	185.9	9.757	3.975
Core TR14 leachate	13L	307	38.847	15.675	18.683	0.83903	2.07933	105.3	9.755	3.962
Core TR14 leachate	6L	330	38.880	15.683	18.706	0.83840	2.07852	98.1	9.767	3.965
Core TR14 leachate	38L	343	38.849	15.677	18.685	0.83905	2.07925	106.1	9.758	3.962
Core TR14 leachate	14L	357	38.888	15.681	18.720	0.83767	2.07726	85.8	9.762	3.960
Core TR14 leachate	1L	382	38.856	15.676	18.697	0.83841	2.07826	95.9	9.754	3.958
Core TR14 leachate	28L	405	38.869	15.679	18.702	0.83840	2.07837	96.7	9.761	3.962
Core TR14 leachate	15L	419	38.861	15.678	18.701	0.83833	2.07799	95.0	9.757	3.959
Core TR14 leachate	26L	434	38.856	15.677	18.691	0.83874	2.07888	101.7	9.757	3.962
Core TR14 leachate	16L	456	38.856	15.680	18.689	0.83899	2.07908	106.6	9.763	3.964
Core TR14 leachate	7L	474	38.844	15.676	18.681	0.83914	2.07928	107.7	9.757	3.962
Core TR14 leachate	17L	539	38.845	15.679	18.680	0.83935	2.07958	111.8	9.762	3.964
Core TR14 leachate	33L	547	38.839	15.677	18.677	0.83940	2.07953	112.0	9.759	3.963
Core TR14 leachate	12L	555	38.836	15.674	18.689	0.83863	2.07798	98.3	9.750	3.954
Core TR14 leachate	27L	570	38.843	15.679	18.685	0.83911	2.07881	108.1	9.762	3.960
Core TR14 leachate	8L	584	38.838	15.674	18.694	0.83850	2.07765	96.3	9.752	3.952
Core TR14 leachate	18L	599	38.840	15.678	18.698	0.83851	2.07720	98.2	9.759	3.952
Core TR14 leachate	35L	647	38.793	15.673	18.643	0.84063	2.08076	130.1	9.753	3.960
Core TR14 leachate	2L	670	38.753	15.677	18.619	0.84198	2.08129	152.2	9.763	3.957
Core TR14 leachate	19L	695	38.748	15.668	18.604	0.84220	2.08276	152.7	9.749	3.961
Core TR14 leachate	30L	706	38.729	15.666	18.589	0.84278	2.08343	161.1	9.746	3.961
Core TR14 leachate	9L	737	38.948	15.685	18.781	0.83512	2.07380	46.4	9.763	3.954
Core TR14 leachate	36L	753	38.781	15.674	18.629	0.84134	2.08170	141.5	9.757	3.963
Core TR14 leachate	10L	771	38.708	15.667	18.562	0.84404	2.08526	180.9	9.751	3.966
Core TR14 leachate	24L	799	38.813	15.677	18.656	0.84029	2.08040	125.8	9.760	3.962
Core TR14 leachate	39L	842	38.999	15.690	18.805	0.83433	2.07383	35.7	9.771	3.963
Core TR14 leachate	11L	892	38.990	15.686	18.801	0.83433	2.07384	33.7	9.764	3.961
Core TR14 residue	34 RR	63	39.004	15.699	18.928	0.82941	2.06062	−40.4	9.778	3.902
Core TR14 residue	20 RR	114	39.018	15.696	18.865	0.83205	2.06835	1.5	9.778	3.941
Core TR14 residue	40 RR	130	39.032	15.701	18.889	0.83121	2.06634	−9.9	9.785	3.935
Core TR14 residue	32 RR	160	39.045	15.705	18.941	0.82915	2.06140	−42.7	9.788	3.913
Core TR14 residue	21 RR	174	39.051	15.702	18.914	0.83014	2.06459	−27.5	9.784	3.929
Core TR14 residue	22 RR	202	39.058	15.700	18.932	0.82924	2.06306	−42.8	9.779	3.922
Core TR14 residue	25 RR	214	39.003	15.700	18.874	0.83183	2.06654	−1.1	9.784	3.930
Core TR14 residue	41 RR	223	39.038	15.702	18.921	0.82984	2.06322	−32.3	9.784	3.920
Core TR14 residue	42 RR	242	38.899	15.682	18.741	0.83680	2.07563	72.2	9.762	3.954
Core TR14 residue	23 RR	257	38.964	15.688	18.777	0.83549	2.07513	53.8	9.770	3.964
Core TR14 residue	5 RR	269	38.904	15.679	18.705	0.83826	2.07994	94.3	9.760	3.975
Core TR14 residue	29 RR	298	38.947	15.684	18.751	0.83638	2.07701	66.4	9.764	3.969
Core TR14 residue	6RR	330	38.979	15.692	18.801	0.83462	2.07328	41.1	9.775	3.958
Core TR14 residue	38 RR	343	38.989	15.690	18.825	0.83347	2.07116	21.9	9.769	3.949
Core TR14 residue	14 RR	357	39.015	15.696	18.831	0.83351	2.07184	24.8	9.780	3.957
Core TR14 residue	28 RR	405	38.935	15.689	18.755	0.83655	2.07602	71.0	9.774	3.963
Core TR14 residue	15 RR	419	38.994	15.692	18.799	0.83472	2.07423	42.8	9.776	3.965
Core TR14 residue	26 RR	434	38.953	15.688	18.763	0.83608	2.07600	63.0	9.770	3.966
Core TR14 residue	7 RR	474	38.936	15.688	18.749	0.83672	2.07669	73.4	9.772	3.967
Core TR14 residue	17 RR	539	38.971	15.692	18.784	0.83534	2.07467	52.9	9.776	3.963

Table S2. Cont.

Material	Code	Depth, cm	$^{208}Pb/^{204}Pb$	$^{207}Pb/^{204}Pb$	$^{206}Pb/^{204}Pb$	$^{207}Pb/^{206}Pb$	$^{208}Pb/^{206}Pb$	T_{mod}, Ma	μ	κ
Core TR14 residue	33 RR	547	38.962	15.688	18.787	0.83508	2.07391	47.4	9.770	3.958
Core TR14 residue	27 RR	570	38.984	15.692	18.814	0.83402	2.07206	31.6	9.774	3.953
Core TR14 residue	18 RR	599	39.018	15.694	18.866	0.83186	2.06817	−2.5	9.774	3.939
Core TR14 residue	35 RR	647	39.001	15.692	18.829	0.83343	2.07140	22.4	9.774	3.952
Core TR14 residue	19 RR	695	39.006	15.696	18.833	0.83341	2.07112	23.7	9.780	3.953
Core TR14 residue	30 RR	706	38.981	15.689	18.812	0.83398	2.07206	30.0	9.769	3.952
Core TR14 residue	9 RR	737	38.994	15.689	18.779	0.83542	2.07645	52.9	9.771	3.975
Core TR14 residue	36 RR	753	38.993	15.695	18.824	0.83379	2.07144	29.1	9.780	3.952
Core TR14 residue	24 RR	799	38.989	15.691	18.789	0.83512	2.07515	49.3	9.775	3.968
Core TR14 residue	39 RR	842	38.889	15.683	18.714	0.83807	2.07819	92.7	9.766	3.965
Core CN1 leachates	55	74	38.793	15.674	18.601	0.84266	2.08557	162.1	9.761	3.984
Core CN1 leachates	56	125	38.903	15.682	18.726	0.83743	2.07747	82.3	9.763	3.964
Core CN1 leachates	57	168	38.765	15.669	18.601	0.84238	2.08402	155.8	9.751	3.970
Core CN1 leachates	58	179	38.817	15.674	18.640	0.84089	2.08247	134.1	9.756	3.972
Core CN1 leachates	59	199	38.802	15.674	18.632	0.84122	2.08254	139.1	9.756	3.970
Core CN1 leachates	60	227	38.883	15.678	18.724	0.83731	2.07658	79.0	9.756	3.956
Core CN1 leachates	61	249	38.928	15.686	18.747	0.83672	2.07651	72.7	9.769	3.964
Core CN1 leachates	62	268	38.916	15.682	18.731	0.83723	2.07769	79.1	9.763	3.967
Core CN1 leachates	63	275	38.907	15.681	18.725	0.83742	2.07774	82.5	9.762	3.966
Core CN1 leachates	64	298	38.903	15.682	18.756	0.83615	2.07422	62.1	9.761	3.948
Core CN1 leachates	65	318	38.912	15.681	18.754	0.83615	2.07485	61.5	9.759	3.952
Core CN1 leachates	66	325	38.861	15.677	18.703	0.83823	2.07782	92.8	9.756	3.957
Core CN1 leachates	67	340	38.890	15.679	18.714	0.83783	2.07820	87.6	9.759	3.965
Core CN1 leachates	68	378	38.918	15.684	18.734	0.83719	2.07741	79.3	9.766	3.967
Core CN1 leachates	69	399	38.869	15.677	18.706	0.83804	2.07785	90.4	9.755	3.959
Core CN1 leachates	70	425	38.889	15.679	18.702	0.83838	2.07944	96.4	9.760	3.971
Core CN1 leachates	71	448	38.854	15.678	18.706	0.83812	2.07710	91.8	9.758	3.953
Core CN1 leachates	72	468	38.892	15.683	18.712	0.83813	2.07849	93.7	9.766	3.967
Core CN1 leachates	73	477	38.869	15.680	18.706	0.83830	2.07800	94.7	9.762	3.960
Core CN1 leachates	74	522	38.882	15.679	18.699	0.83853	2.07938	99.1	9.761	3.969
Core CN1 leachates	75	532	38.751	15.671	18.572	0.84378	2.08649	178.6	9.758	3.981
Core CN1 leachates	76	553	38.550	15.662	18.379	0.85216	2.09741	303.7	9.761	3.998
Core CN1 leachates	77	583	38.666	15.664	18.511	0.84622	2.08880	213.5	9.751	3.976
Core CN1 leachates	78	651	38.681	15.665	18.531	0.84533	2.08738	200.3	9.749	3.972
Core CN1 leachates	79	684	38.957	15.686	18.809	0.83398	2.07116	28.6	9.764	3.943
Core CN1 leachates	80	741	38.908	15.687	18.717	0.83813	2.07876	95.7	9.775	3.972
Core CN1 leachates	81	791	38.965	15.686	18.802	0.83422	2.07233	32.7	9.763	3.950
Core CN1 leachates	82	834	38.985	15.691	18.812	0.83409	2.07232	32.3	9.772	3.954
Core CN1 leachates	83	891	38.957	15.690	18.828	0.83332	2.06913	19.5	9.768	3.933
Core CN1 leachates	84	925	38.951	15.684	18.819	0.83337	2.06964	18.1	9.758	3.934
Core CN1 leachates	85	975	38.941	15.686	18.805	0.83414	2.07076	31.2	9.764	3.938
Core CN1 leachates	86	1,042	38.942	15.688	18.832	0.83305	2.06784	14.1	9.765	3.925
Core CN1 leachates	88	1,076	38.962	15.688	18.813	0.83388	2.07101	27.4	9.766	3.943
Core CN1 leachates	87	1,125	38.956	15.685	18.807	0.83399	2.07137	28.7	9.762	3.943
Core CN1 leachates	89	1,179	38.950	15.685	18.805	0.83406	2.07122	29.5	9.762	3.942
Core CN1 leachates	90	1,225	38.959	15.687	18.801	0.83435	2.07217	34.7	9.765	3.948
Core CN1 leachates	91	1,262	38.946	15.685	18.810	0.83387	2.07046	26.7	9.762	3.937
Modern Tiber bedload	TA 2–117		38.717	15.667	18.558	0.84425	2.08632	184.2	9.751	3.973
Modern Tiber bedload	TA 3–118		38.646	15.662	18.496	0.84674	2.08938	221.3	9.747	3.975
Modern Tiber bedload	TA 4–119		38.630	15.660	18.487	0.84708	2.08947	225.5	9.746	3.972
Modern Tiber bedload	TA 1–120		38.732	15.668	18.577	0.84339	2.08488	171.4	9.751	3.969
Modern Tiber bedload	DF 1–122		38.679	15.665	18.540	0.84493	2.08622	193.8	9.748	3.966
Modern Tiber bedload	F 2–121		38.676	15.666	18.529	0.84552	2.08733	203.5	9.753	3.971
Roman lead pipe	LP 1		38.602	15.657	18.475	0.84748	2.08944	230.5	9.740	3.966
Roman lead pipe	LP 2a		38.585	15.660	18.465	0.84803	2.08947	240.0	9.746	3.964
Roman lead pipe	LP 2b		38.582	15.656	18.463	0.84799	2.08979	238.1	9.740	3.964
Roman lead pipe	LP 2c		38.596	15.657	18.463	0.84800	2.09042	238.3	9.741	3.970
Roman lead pipe	LP 2d		38.606	15.660	18.466	0.84805	2.09065	239.9	9.747	3.973
Roman lead pipe	LP 3a		38.620	15.659	18.478	0.84747	2.09006	230.8	9.744	3.973
Roman lead pipe	LP 3b		38.658	15.661	18.506	0.84626	2.08889	212.3	9.744	3.974
Roman lead pipe	LP 3c		38.664	15.663	18.510	0.84621	2.08877	213.0	9.749	3.975
Roman lead pipe	LP 4		39.018	15.688	18.710	0.83852	2.08542	102.2	9.777	4.023
Roman lead pipe	LP 5		38.590	15.654	18.462	0.84794	2.09024	236.6	9.737	3.968